PERGAMON

Solid State Communications 118 (2001) 85–90

solid state communications

www.elsevier.com/locate/ssc

# Influence of the electrolyte viscosity on the structural features of porous silicon

M. Servidori[a,*], C. Ferrero[b], S. Lequien[c], S. Milita[a], A. Parisini[a], R. Romestain[d], S. Sama[a], S. Setzu[d,e], D. Thiaudière[f,g]

[a]*CNR-Istituto LAMEL, Via P. Gobetti 101, 40129 Bologna, Italy*
[b]*European Synchrotron Radiation Facility, BP 220, 38043 Grenoble Cedex, France*
[c]*Laboratoire Pierre Sue, CEA-CNRS, CEN Saclay, 91191 Gif sur Yvette, France*
[d]*Laboratoire de Spectrométrie Physique, BP 87, 38402 St. Martin d'Hères Cedex, France*
[e]*Physics Department, Cagliari University, 09042 Monserrato, Italy*
[f]*Centre de Recherche sur les Matériaux à Haute Température, 1d Av. de la Recherche Scientifique, 45071 Orléans Cedex, France*
[g]*Laboratoire pour l'Utilisation du Rayonnement Electromagnétique (LURE), 91898 Orsay Cedex, France*

Received 28 September 2000; received in revised form 9 January 2001; accepted 24 January 2001 by J.F. Sadoc

**Abstract**

The influence of an increase in the electrolyte viscosity, obtained by reducing the chemical bath temperature, replacing a volume fraction of ethanol with the heavier glycerol and increasing the anodization current density, was studied in porous silicon layers formed on p-type silicon. Synchrotron X-ray reflectivity and cross-sectional transmission electron microscopy techniques were used for 300-nm-thick porous silicon layers. For greater thicknesses (10 μm), the temperature effect was investigated by multicrystal X-ray diffraction with a laboratory source. It was found that higher average porosities and lower roughnesses at the interface between porous silicon and substrate are obtained when the electrolyte viscosity increases. Moreover, the formation of flatter porosity depth-profiles is favored by lowering the electrolyte temperature. The importance of these effects on the performances of optical devices based on porous silicon is underlined. 

*Keywords:* A. Porous materials; C. X-ray scattering; E. Synchrotron radiation

*PACS*: 61.43.Gt; 61.10.Kw; 61.16.Bg

## 1. Introduction

Porous silicon (PS) is nowadays a very attractive material for manufacturing silicon on insulator structures [1], optical devices [2,3] and solid-state chemical microsensors [4]. The wide field of applications is due to the fact that the properties of the material are very dependent on the type and resistivity of the starting silicon (Si) substrate and on the electrochemical parameters used for the anodization process. These latter are essentially the composition of the electrolyte (HF, $H_2O$ and alcohol), the current density $J$ and the chemical bath temperature $T$.

In recent papers [5,6] the influence of $J$ and $T$ on the porosity and PS–Si interface roughness was studied by weighing, optical, and mechanical techniques in p-type samples having PS thicknesses $\geq 5$ μm. It was found that an increase in $J$ produces higher porosities and flatter interfaces between PS and Si, and that, for given $J$ and electrolyte composition, a decrease in $T$ from room temperature to $-31$°C reduces remarkably the PS–Si interface roughness. The temperature effect was ascribed to an increase in the electrolyte viscosity which favors asperity smoothening under anodization regime tending to electropolishing [7]. The same behavior was observed when a volume fraction of the ethanol is replaced by a heavier (more viscous) alcohol like glycerol [6]. However, in those investigations the authors determined average porosity values by gravimetric measurements, thereby losing information on the porosity

* Corresponding author. Tel.: +39-051-639-9184; fax: +39-051-639-9216.

*E-mail address:* servidori@lamel.bo.cnr.it (M. Servidori).

0038-1098/01/$ - see front matter 
PII: S0038-1098(01)00036-9

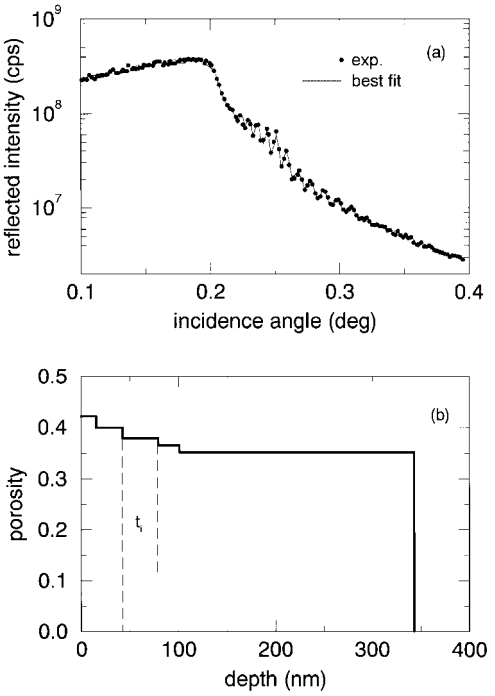


Fig. 1. (a) Experimental (full circles) and calculated (line) XRR spectra taken with 7.1 keV synchrotron X-rays from sample 2 in Table 1. (b) Porosity profile resulting from the best fit in (a).

depth-profile, as these measurements require chemical removal of the PS layer in sodium hydroxide solution.

In this work the influence of $J$, $T$ and 10% substitution of ethanol with glycerol on porosity, interface roughness and porosity depth-profile is studied. Synchrotron X-ray reflectivity (XRR) spectra and cross-sectional transmission electron microscopy (XTEM) images were taken from 300-nm-thick PS layers formed on p-type Si substrate. Moreover, rocking curves (RCs) were obtained by multicrystal X-ray diffraction (MCXRD) from 10 μm PS thickness on p-type Si to verify the influence of $T$ on the porosity depth-gradient in thick layers. All these aspects are very important in the field of PS-based optical devices.

## 2. Experimental

PS layers with nominal thicknesses of 300 nm were prepared by anodizing in the dark p-type (boron doping, 8–9 Ω cm resistivity) Si substrates in a solution of HF/$H_2O$/ethanol = 35:35:30. The $J$ values were 16.6, 166 and 333 mA/cm$^2$, and $T = 24$ or $-31$°C was used for anodization with $J = 16.6$ mA/cm$^2$. For each of the three $J$ values, 10% of ethanol was replaced by glycerol. Moreover, 10-μm-thick PS layers were formed on doped Si at $T = 24$ or $-31$°C using $J = 16.6$ mA/cm$^2$ without glycerol.

XRR measurements were made at the ID1 beamline of the European Synchrotron Radiation Facility (ESRF) in Grenoble (France). The energy of 7.1 keV was selected by a pair of Si crystals oriented in $(n, -n)$ 311 symmetric Bragg-case diffraction, and a single 111 symmetric reflection Si analyzer was placed downstream the sample to prevent the detector from collecting the strong diffuse X-ray scattering from the porous structure. The beam diameter at the sample was reduced to 50 μm by means of slits. Longitudinal specular XRR scans were obtained from 300-nm-thick PS by rotating sample and analyzer in $\theta/2\theta$ coupling, and the measurements were simulated by a computer code based on optical multislice theory [8] which takes multiple scattering into account. From the best fit, obtained by routines of minimization between experiment and calculation, layer thickness, porosity profile, roughnesses at the PS–air and PS–Si interfaces were determined.

XTEM observations were performed at LAMEL Institute with a Philips CM30-T microscope operating at 300 kV. The instrument was equipped with a Gatan 794 multiple scan camera allowing digital image recording on a $1024 \times 1024$ pixel charge coupled device array.

MCXRD measurements were made at the Laboratoire de Spectrométrie Physique (LSP) with a Philips MRD

Table 1
PS thickness ($t$) and interface roughness ($\sigma$) obtained from XRR measurements and XTEM observations as a function of the current density ($J$), the electrolyte temperature ($T$) and the glycerol percent. Discrepancies among some of the $t$ and $\sigma$ values obtained from XRR and XTEM are evident (see text for details)

| Sample | $J$ (mA/cm$^2$) | $T$ (°C) | Glycerol (% vol) | $t_{XRR}$ (nm) | $t_{XTEM}$ (nm) | $\sigma_{XRR}$ (nm) | $\sigma_{XTEM}$ (nm) | $\bar{p}$ (%) |
|---|---|---|---|---|---|---|---|---|
| 1 | 16.6 | 24 | 0 | | 303 ± 6 | | 28 ± 2 | |
| 2 | 16.6 | 24 | 10 | 343 ± 4 | | 7.9 ± 0.5 | | 36.2 ± 0.4 |
| 3 | 166 | 24 | 0 | 324 ± 4 | 331 ± 6 | 13.6 ± 0.5 | 10 ± 2 | 37.5 ± 0.4 |
| 4 | 166 | 24 | 10 | 369 ± 4 | 354 ± 7 | 6.7 ± 0.5 | 9 ± 2 | 39.8 ± 0.5 |
| 5 | 333 | 24 | 0 | 386 ± 4 | | 4.8 ± 0.5 | | 40.0 ± 0.4 |
| 6 | 333 | 24 | 10 | 402 ± 4 | 373 ± 8 | 5.8 ± 0.5 | 5 ± 2 | 45.0 ± 0.6 |
| 7 | 16.6 | − 31 | 0 | 269 ± 3 | | 5.7 ± 0.5 | | 37.9 ± 0.4 |
| 8 | 16.6 | − 31 | 10 | 267 ± 3 | 256 ± 5 | 4.9 ± 0.5 | 5 ± 2 | 38.2 ± 0.5 |

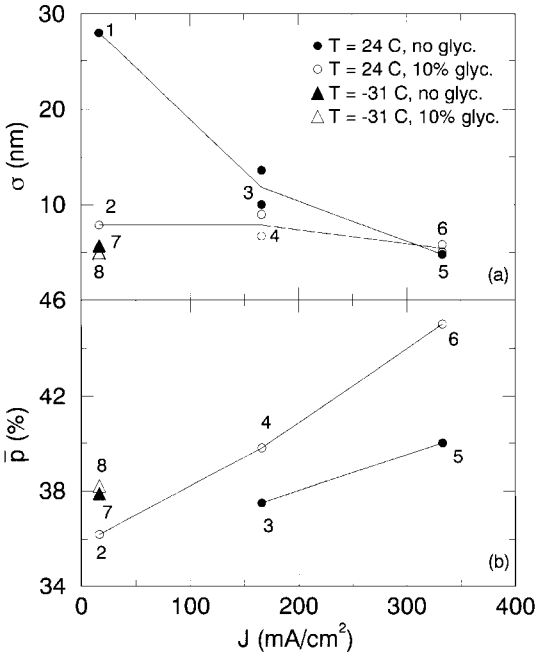


Fig. 2. Interface roughness (a) and average porosity (b) vs anodization current density for the two different electrolyte temperatures and alcohol compositions. The sample numbers are reported near the respective symbols. The lines are guides to the eye.

diffractometer installed at a conventional Cu $K\alpha_1$ source. The instrument was equipped with a two-crystal, four-reflection (220) germanium monochromator. RCs were obtained from 10-μm-thick PS and were reproduced by a dynamical diffraction code developed for implanted Si layers [9], suitably modified to take into account the reduction by porosity of the Fourier coefficients of $4\pi$ times the Si polarizability [10]. The depth profiles of porosity ($p$) and perpendicular lattice mismatch ($m_\perp$) between PS and substrate were determined by the same minimization routines used for the simulations of the XRR spectra, and were found to be linearly related to each other, according to what was already observed [11].

All the samples were anodized at LSP and measured by XRR and MCXRD just after the anodization. Some weeks later, a few of them were thinned for XTEM observations.

## 3. Results

Fig. 1a shows the experimental (dots) and calculated (line) XRR profiles taken from a sample anodized with electrolyte composition $HF/H_2O$/ethanol/glycerol = 35:35:20:10, $J = 16.6$ mA/cm$^2$ and $T = 24$°C. Two intensity decays are observed at incidence angles of about 0.20 and 0.25°, corresponding to the critical angles for total external reflection of PS layer and Si substrate, respectively, at 7.1 keV X-ray energy. The $p$ profile resulting from the best fit of Fig. 1a is reported in Fig. 1b, where a depth gradient is evident. The low fringe contrast observed in Fig. 1a is mainly due to the roughness at the PS–Si interface ($\sigma$) and in part also to the porosity gradient. The influence of the two parameters on the shape of XRR spectra can be verified by theoretical calculations, which show that a flat $p$ distribution with $\sigma = 0$ gives rise to a high fringe visibility all over the range of incidence angles. By increasing $\sigma$, this visibility is smoothed out only in the high angle region of the XRR spectrum, while a porosity gradient lowers the fringe contrast also at low angles. Thanks to the minimization routines, the correct $p$ profile and $\sigma$ value are then obtained.

The PS thickness ($t$) and the PS–Si interface roughness resulting from the simulation of the experimental XRR spectra and from XTEM intensity profile measurements are summarized in Table 1 as a function of $J$, $T$ and glycerol percent. In the last column, the values of the average porosity $\bar{p} = \sum_i p_i t_i / \sum_i t_i$ are reported, where $i$ is the index of each layer in which the whole PS thickness was divided (Fig. 1b) and $p_i$ is the porosity within each layer of thickness $t_i$. The roughness values determined by XRR at the PS–air interface are not shown in Table 1, as an almost constant value of about 2 nm was obtained irrespective of changes in the anodization parameters. The XRR data for all the samples but sample 1 are reported in Table 1. This was due to an unexpected and fast aging phenomenon observed for PS under the synchrotron beam. The need to obtain reliable spectra from stable samples required so many sample alignment procedures and XRR measurement collections as to exceed the time allocated at ESRF for all the planned experiments. As will be described elsewhere [12], the PS aging was the reason why the $\bar{p}$ values in Table 1 are remarkably lower than the average porosities of 0.55–0.75 reported in Refs. [5,6] for samples anodized under the same experimental conditions.

Discrepancies among some of the $t$ and the $\sigma$ values obtained from XRR measurements and XTEM images are evident in Table 1. These might arise from the much larger sample surface probed by XRR in comparison with that imaged by XTEM. However, the overall agreement is satisfactory at exception of the $t$ values for sample 6. In the case of sample 6, both techniques give a low $\sigma$ value, i.e. a nearly flat PS–Si interface, indicating that the discrepancy cannot be attributed to the effects of local roughness variations on the $t$ values determined by XTEM imaging a small portion of the sample. More probably, at the origin of this disagreement are two main reasons. On the one hand, in XTEM intensity profile measurements, small systematic errors in the determination of the PS layer thickness could be possible owing to the presence of a Fresnel fringe at the interface between PS and the denser Si region. On the other hand, due to the grazing geometry of XRR measurements, surface regions close to the rim of PS layer, where inhomogeneities are expected, can contribute to the measured spectra.

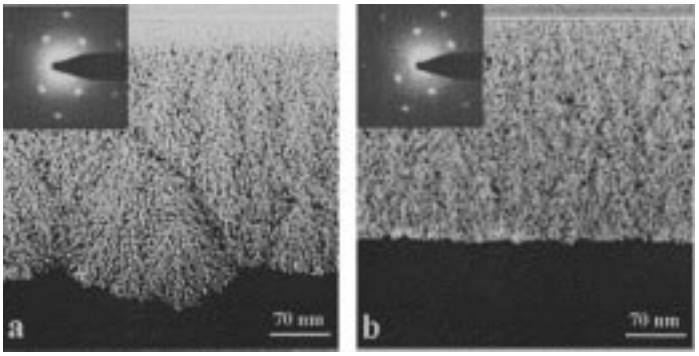


Fig. 3. XTEM images and SAED patterns (insets) taken from sample 1 (a) and sample 8 (b).

To comment upon the XRR and XTEM results in easier way, the $\sigma$ and $\bar{p}$ data of Table 1 are plotted in Fig. 2 as a function of $J$ for the two temperatures and alcohol compositions. The general picture can be described as follows:

1. *PS–Si interface roughness* (Fig. 2a). Anodizations at room $T$ without glycerol lead to well observable $\sigma$ decreasing with increasing $J$ (samples 1, 3, 5). For given $J$, the $\sigma$ reduction produced by glycerol is more marked the lower $J$ is (samples 1, 2 and 3, 4) and is comparable with the flattening effect due to the increasing in $J$ (samples 5, 6). Anodizations at low $T$ and the lowest $J$ involve a further, though modest, $\sigma$ reduction to the same value measured at the highest $J$, independently of the alcohol composition in the electrolyte (samples 7, 8).
2. *Average porosity* $\bar{p}$ (Fig. 2b). For anodizations performed at room $T$, $\bar{p}$ increases with $J$ and the increase is faster when the electrolyte contains glycerol (samples 2, 4, 6). For low anodization $T$ at the lowest $J$, an enhancement in $\bar{p}$ is observed (sample 7), whereas the 10% replacement of ethanol with glycerol does not lead to an appreciable further increase in $\bar{p}$ (sample 8).

It is worth underlining that, though the values of $\bar{p}$ are considerably lowered as a consequence of the aging phenomenon mentioned above, the trends of $\bar{p}$ and $\sigma$ with $J$, $T$ and glycerol percent follow those already observed in Refs. [5,6] for a much greater PS thickness $t \geq 5$ μm.

The strong difference in $\sigma$ is clearly evidenced in the XTEM phase contrast micrographs of Fig. 3a and b, relative to sample 1 and sample 8, respectively. We can also observe the typical feature of particle-like Si regions (black dots in Fig. 3a and b) in PS formed on p-type Si substrate. However, in the case of sample 1 (Fig. 3a), a tendency to an alignment of the Si particles along filaments is observed in the region close to the Si substrate, clearly indicating that a porosity gradient is present in this sample. In the case of sample 8 (Fig. 3b), this tendency appears to be less pronounced indicating a more homogeneous pore morphology in the PS layer. The crystalline nature of the Si particles is evidenced in the selected area electron diffraction patterns (SAED) taken in PS regions close to the sample surface and reported in the insets to these figures.

As to the porosity depth-profiles obtained in the different experimental conditions, we report the data relative to the effects of $J$ for the samples 2 and 6 (Fig. 4) and $T$ for the

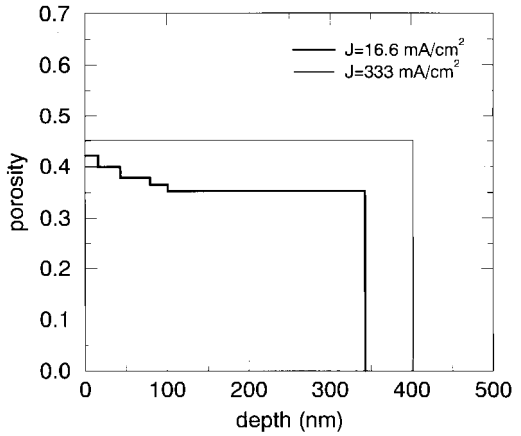


Fig. 4. Porosity profiles obtained from samples 2 and 6 in Table 1.

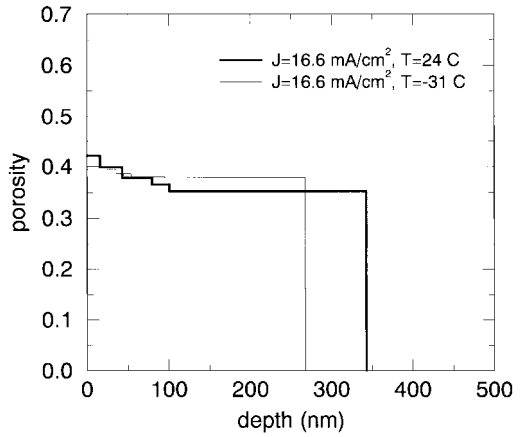


Fig. 5. Porosity profiles obtained from samples 2 and 8 in Table 1.

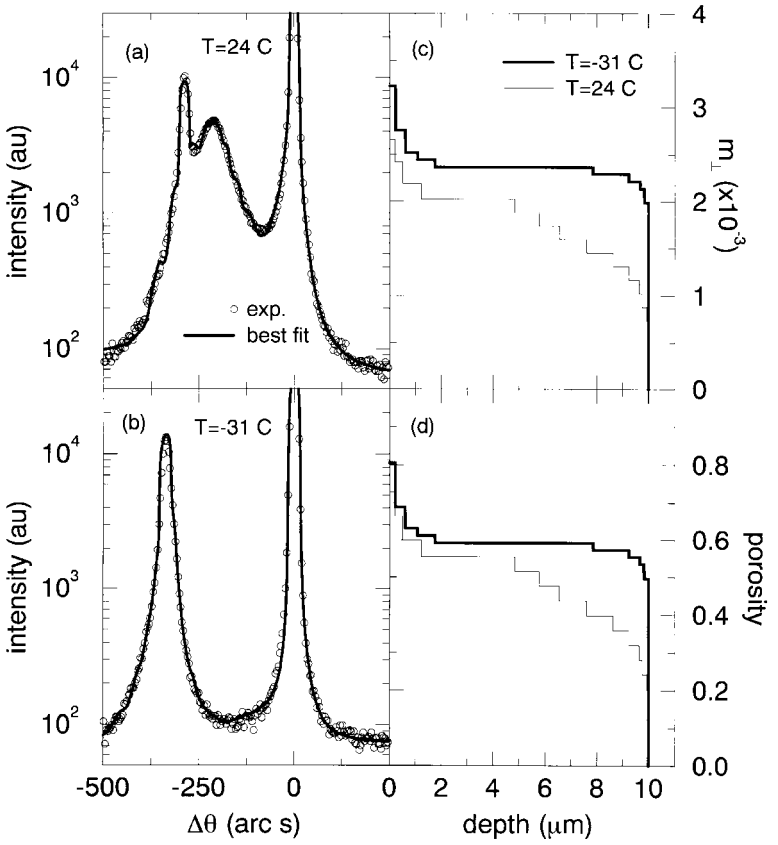


Fig. 6. Experimental (open circles) and calculated (line) RCs for a 10-μm-thick PS formed with $J = 16.6$ mA/cm$^2$ at $T = 24$ (a) and $-31$°C (b). Depth profiles of the perpendicular lattice mismatch between PS and Si substrate (c) and porosity (d) resulting from the best fits in (a) and (b).

samples 2 and 8 (Fig. 5). In both figures, the gradient in the $p$ depth-distribution decreases with increasing $J$ and reducing $T$.

The phenomenon of gradient variation as a consequence of a change in $T$ was investigated also for 10 μm PS thicknesses by MCXRD technique. Fig. 6a and b show the experimental RCs (circles) obtained with $J = 16.6$ mA/cm$^2$ for $T = 24$ and $-31$°C, respectively. In both spectra, the substrate peak at the reference angle $\Delta\theta = 0$ and an intensity contribution given by PS at lower angles are present. The PS intensity profiles are quite different for the different $T$, consisting of a double peak for $T = 24$°C and a single peak for $T = -31$°C. To extract quantitative information, the RCs were simulated by constraining the whole $m_\perp$ and $p$ profiles to be confined within the nominal 10 μm thickness. This constraint is imposed by the fact that for a very thick epilayer of even constant $m_\perp$, the angular frequency of the intrinsic intensity oscillations in the RC, driving the diffraction code towards the determination of the surface layer thickness, is so narrow as to be completely smoothed out by the angular divergence in the diffraction plane and the wavelength dispersion of the beam exiting the monochromator. An additional blurring effect is given by possible depth gradients of $m_\perp$. As can be seen in Fig. 6c and d, larger gradients in the $m_\perp$ and porosity profiles are produced by the higher $T$, underlining again the beneficial effect produced by lowering $T$. The comparison between Figs. 5 and 6d indicates that this effect is not only preserved but also enhanced in thicker PS. The surface peaks observed in the $m_\perp$ and $p$ profiles of Fig. 6c and d, respectively, are very probably due to pore size widening induced by the prolonged anodization time necessary to form thick PS layers and/or by Si skeleton consumption associated with the beginning of post-anodization PS oxidation to air. As a final remark, an average porosity $\bar{p} = 0.59 \pm 0.05$ results from the $p$ profile in the sample anodized at $T = -31$°C (Fig. 6d). This value is much higher than that of sample 8 in Table 1 and agrees well with the one expected from the used anodization conditions [5,6] in the absence of aging. This suggests that the aging phenomenon under laboratory X-rays is not so fast as that observed at the ID1 beamline of ESRF.

## 4. Discussion and conclusions

This paper deals with the influence of some anodization parameters (current density, electrolyte temperature and percent of ethanol-replacing glycerol in the chemical bath) on the macroscopic structural characteristics of single PS layers formed on p-type Si substrates. It was already observed [5,6] that increasing $J$ and glycerol percent, and decreasing $T$ produce PS layers with higher porosity and lower roughness at the interface with the substrate. In addition to this, the present paper shows that a lowering in $T$ favors the formation of flatter porosity depth-profiles. These effects are linked to an increase in the electrolyte viscosity, which results from lowering $T$, as well as replacing part of ethanol with the heavier glycerol. As to the effect of $J$, this can be interpreted as a manifestation of a limited diffusion of the chemical species which becomes more apparent when the reaction is driven on a shorter timescale by increasing the current density. Indeed, it is generally admitted that above a critical current density electropolishing prevails above pore formation [7]. Therefore, in an electrolytic regime of viscosity-induced limited diffusion, higher porosities, more homogeneous porosity depth-profiles and flatter interfaces are obtained.

Good structural characteristics of PS are very important from the point of view of optical devices. For instance, light transmission in PS-based waveguides can undergo severe losses through diffuse scattering at interface roughnesses [13,14] and have perturbed propagation modes owing to different optical refractive indices associated with porosity depth-gradients. As described in this work, these detrimental behaviors can be removed by choosing appropriate anodization parameters.

In previous papers [5,6] quite different optical refractive indices were measured in PS layers having the same average porosity, though obtained with different $J$ and $T$ values. To account for this result, the hypothesis was made that pores of different sizes are formed in the layers. This hypothesis will be verified in a subsequent paper [15], where results of grazing incidence small angle X-ray scattering (GISAXS) measurements made at the ESRF-ID1 beamline will be reported. The GISAXS data were taken from the same samples investigated here, immediately after the XRR measurements.

## References

[1] G. Bomchil, A. Halimaoui, R. Herino, Microelectron. Engng 8 (1988) 293.
[2] M.G. Berger, S. Frohnhoff, W. Theiss, U. Rossow, H. Muender, Porous Silicon Science and Technology, Springer, New York, 1994, p. 345.
[3] A. Loni, L.T. Canham, M.G. Berger, R. Arens-Fisher, H. Muender, H. Luth, H. Arrand, T.M. Benson, Thin Solid Films 276 (1996) 143.
[4] P. Maccagnani, L. Dori, P. Negrini, Proc. Eurosensor XIII Conference, The Hague, 1999, p. 817.
[5] S. Setzu, G. Lérondel, R. Romestain, J. Appl. Phys. 84 (1998) 3129.
[6] S. Setzu, PhD thesis, Université J. Fourier, Grenoble, France, 1999.
[7] D.R. Turner, J. Electrochem. Soc. 105 (1957) 402.
[8] L.G. Parrat, Phys. Rev. 95 (1954) 359.
[9] M. Servidori, F. Cembali, S. Milita, X-Ray and Neutron Dynamical Diffraction: Theory and Applications, Series B: Physics, vol. 357, Plenum Press, New York, 1996 (p. 301).
[10] A.A. Lomov, D. Bellet, G. Dolino, Phys. Status Solidi (B) 190 (1995) 219.
[11] D. Bellet, G. Dolino, Thin Solid Films 276 (1996) 1.
[12] S. Sama, C. Ferrero, S. Lequien, S. Milita, R. Romestain, M. Servidori, S. Setzu, D. Thiaudiere, J. Phys. D: Appl. Phys. (2001) in press.
[13] G. Lérondel, R. Romestain, F. Madéore, F. Muller, Thin Solid Films 276 (1996) 80.
[14] G. Lérondel, R. Romestain, Thin Solid Films 297 (1996) 114.
[15] M. Servidori et al., in preparation.